NAVIER STOKES COMPUTATIONS ON A TWIN ENGINE NOZZLE-AFTERBODY

A. Gogoi & S. Sundaramoorthi
Aeronautical Development Agency
Post Box 1718, Vimanapura,
Bangalore 560 017, India
agogoi@yahoo.com

Abstract

The report presents turbulent Navier Stokes computations on twin engine afterbody model with jet exhaust. The computations are carried out for free-stream Mach number of 0.8 to 1.20 and jet pressure ratio of 3.4 to 7.8. The Spalart-Allmaras turbulence model is used in the computations. Comparison is made with experimental data and Cp distribution around the afterbody is found to agree well with experiments. Flow features of the exhaust jet like under expansion, over expansion, Mach discs, etc are well captured. The effect of nozzle pressure ratio and flight Mach number are studied in detail. These computations serve as validation of the in-house code for twin jet afterbody.

Introduction

The flow around the afterbody of fighter aircraft is extremely complex and prone to separation. The afterbody contributes a significant portion of the overall drag of the aircraft. The exhaust jets also have considerable effect of the flow around the afterbody. The relative position of the two engines in twin-engine aircrafts has a considerable effect on the total drag of the aircraft. Therefore, efficient integration of engine nozzle with aircraft afterbody is essential in order to reduce the total drag of aircraft and also obtain maximum output from the propulsion system.

Thus in the present work turbulent Navier-Stokes computations are carried out on a twin jet nozzle-afterbody test case using a in-house code.

Solver Details

The in-house code NUMBERS (NUmerical Multi Block Euler and RANS Solver) is an upgraded version of earlier code VASBI-2 which was meant for isolated intake ducts. The code NUMBERS solves the Euler and Reynolds Averaged Navier-Stokes equation in the compressible flow regime. The code NUMBERS is a multi purpose one and complex geometries are handled by means of structured multi-block grids. Information about the neighboring block number, its face number, orientation and extend is required as input for calculating the neighbors of the cells at the block boundaries. The turbulence is modeled by the algebraic Baldwin-Lomax model or the one-equation Spalart-Allmaras model [/4/] . The equations can be solved by the predictor-corrector MacCormack scheme, central-difference Jameson-Schmidt-Turkel scheme [/5/] or the upwind Convective Upwind Split Pressure (CUSP) scheme [/6/] . Boundary conditions like inflow, outflow, free stream, slip, no-slip, symmetry plane and singular lines are implemented in the code.

The code has been previously validated on the nozzle-afterbody test case of Reubush-Runckel [/2/] and used to obtain solutions on single engine nozzle-afterbody configurations of fighter aircrafts [/1/].

Geometry Modeling and Grid Generation

The geometry of the test case is shown in figure 1 and a schematic of the test case is shown in figure 2 [/2/]. The various circumferential location of the pressure orifices are shown in figure 3. The geometry modeling and grid generation are carried out in software IGG of NUMECA. The grid is a multi-block one comprising of four blocks with a total of 1,265,664 finite volumes. The first block has a size of 97×65×65 points and represents the fore-body. The second block has a size of 97×65×65 and represents the afterbody and the boat-tail. The third block has a size of 73×65×65 and comprise of the region downstream of the nozzle. The fourth block has a size of 73×41×65 and represents the nozzle. The surface grid is shown in figure 4 and a zoomed up view of the grid near the nozzle-afterbody is shown in figure 5. It can be seen from figure 5 that the grid has desirable feature of orthogonality and clustering near the walls. The vertical and horizontal tails are not used in the present work and shall be incorporated in future work. The details of the grid are described in Table 1.

Table 1: Grid Description

Block No	Grid Size	Description
1	97× 65 × 65	Forebody Region
2	97× 65 × 65	Afterbody Region
3	73× 65 × 65	Exhaust Jet Region
4	73× 41 × 65	Nozzle Region

Computational Details

The in-house code is used for obtaining solutions on the twin-jet nozzle–afterbody. The NS equations are solved by a Jameson-Schmidt-Turkel scheme [/5/]. The one-equation Spalart-Allmaras model [/4/] is used in the computations since the Baldwin-Lomax model is known to be unsuitable for free shear flows like jets.. The computations are carried out on Linux based, HP Intel Xeon 2.4 GHz workstations. The freestream total pressure and total temperature were taken as 101325 Pa

and 288.15 K. The computations are carried out at freestream Mach numbers of 0.8, 0.9 and 1.2 at a nozzle pressure ratio of 3.4 which is close to the fully-expanded nozzle pressure ratio of 3.54. Computations are also carried out at a high nozzle pressure ratio of 7.8. The Reynolds number for the computations varied from about 19 million to 22 million. CFL number of 2.5 is used in the computation which is very close to the limit of 2.8 for the four step integration scheme. The constants for second order and fourth order dissipation terms of the JST scheme are taken as 1/2 and 1/20 respectively.

The computations are described in Table 2. The CPU time for 5000 iterations on medium grid was about 48 minutes while the CPU time for 5000 iterations on fine grid was about 215 minutes.

Table 2: Details of Computations

S.No	Mach number	Nozzle Pressure Ratio, (NPR)	Angle of Attack (AOA), Degrees	Reynolds number
1	0.80	3.40	0	19,335,952
2	0.90	3.40	0	23,341,492
3	1.20	3.40	0	22,852,732
4	0.80	7.92	0	19,335,952
5	0.90	3.40	8	23,341,492
6	1.20	7.83	0	22,852,732

Results

C_P Plots

The static pressure coefficient, Cp, on the afterbody and boattail surface at various circumferential locations (θ = 0, 180, 225, 240, 255, 270 and 285 degrees) for Mach 0.8, 0.9 and 1.2 are plotted in figure 6, 7 and 8 respectively. The experimental data are taken for the mid location of horizontal tail and forward location of vertical tail. Comparison with experimental data is found reasonable for the all cases. Agreement with experimental data is best for $\theta = 225^o$, $\theta = 240^o$ and $\theta = 255^o$ for all the cases. This may be due to the fact that the effect of the vertical and horizontal tails are negligible in these regions. Similarly, the large differences between the experimental and computed results at $\theta = 0^o$ may be due to the presence of the vertical tail which are not modeled in the present work.

Mach number Plots

The Mach number plot at the symmetry plane for Mach 0.8, 0.9 and 1.2 at NPR=3.4 and $\alpha = 0$ are shown in figure 9. The acceleration of the flow inside the nozzle can be seen from the figures. The expansion fans and compression shocks inside the nozzle can be seen from the figures. The well known 'Mach Discs' are also seen in the plots, especially for the under-expanded cases (NPR~7.8). Thick boundary layer is observed in the afterbody region for all the cases. An oblique shock in observed in the afterbody region for the supersonic case (M=1.2).

Turbulent Viscosity Plots

The jet flows are known to be highly turbulent and therefore the turbulent viscosity plots (μ_T/μ_L) for the various computations are shown in figure 10. It is observed that turbulent viscosity is about 5000 times the laminar or molecular viscosity in the mixing region of the jet with the free-stream air. The increase in turbulent viscosity is a characteristic feature of mixing flows which is well captured by the Spalart-Allmaras turbulence model used in the present computations. It is also observed that the turbulent viscosity is negligible in the 'potential core' region of the jets at all speeds. The turbulent viscosity is also significant in the afterbody region where strong adverse pressure gradients are encountered.

Effect of Nozzle Pressure Ratio

The effect of nozzle pressure ratio was studied at Mach numbers of 0.8 and 1.2. The comparison of C_P at different nozzle pressure ratios for Mach 0.8 and Mach 1.2 are shown in figures 11 and 12 respectively. The effect of nozzle pressure ratio at Mach 0.8 is found to extend upto 15% of the aircraft model while at Mach 1.2 the effect of nozzle pressure ratio is found to extend upto 5% of the aircraft model. It can be seen that there is increase in C_P on the boattail and afterbody with increase in nozzle pressure ratio. Thus it can be said that nozzle pressure ratio has a significant influence on afterbody drag, especially at subsonic speeds.

Drag Estimation

The afterbody pressure drag coefficient is estimated by the following formula

$$C_D = \frac{1}{q_\infty A_m} \sum_{j=1}^{j=jmax-1} \sum_{k=kstart}^{k=kend} \left(P - P_\infty\right) dA$$

where

j is the grid cell along the circumferential direction

kstart and kend are the start and end of the boat-tail grid cells along the axial direction

dA is the projected area of the grid cell along the axial direction

For the purpose of estimating afterbody drag, It is assumed that the afterbody begins from X=47.26 inch (X/L=0.7). Further, the static pressure measurements were taken from X/L~0.7 onwards by Wing [3]. It is seen from the table that the afterbody drag at supersonic speed is about four times more than the afterbody drag at subsonic speeds (0.8-0.9). Further, afterbody drag is found to reduce with increase in nozzle pressure ratio which is due to the pressurization of the external nozzle surface by the plume which becomes larger with

increase in nozzle pressure ratio.

Table 3 Afterbody Pressure Drag Coefficient

S.No	Mach number	Nozzle Pressure Ratio (NPR)	Afterbody Pressure Drag Coefficient
1	0.80	3.40	0.021524
2	0.90	3.40	0.027202
3	1.20	3.40	0.118970
4	0.80	7.92	0.012162
5	1.20	7.83	0.090217

Conclusion

Turbulent Navier-Stokes computations are carried out on a twin-jet nozzle-afterbody test case using in-house code NUMBERS. The static pressure distribution on the afterbody agrees well with experiments. The flow features like expansion fan, compression shocks and Mach Discs in the jet, static pressure drop and recovery in the boattail, thick boundary layer in the afterbody, high level of turbulence in mixing region are well captured by the code.

Therefore, It can be concluded that the in-house code NUMBERS is capable of simulating complex nozzle-afterbody flows of twin-engine configurations.

References

1. A. Gogoi & K.V.L. Rao, "Navier Stokes Computations on Nozzle-Afterbody Configurations", ISABE-2003-1103, XV ISABE Conference, Cleveland, Ohio, USA, September 2003.
2. David E. Reubush and Jack F. Runckel, “Effects of Fineness Ratios on the Boat-tail Drag of Circular-Arc Afterbodies having Closure Ratios of 0.50 with Jet Exhaust at Mach Number up to 1.30”, Report No NASA TN D-7162.
3. David J. Wing, " Afterbody/Nozzle Pressure Distributions of a Twin-Tail, Twin-Engine Fighter with Axisymmetric Nozzles at Mach Numbers from 0.6 to 1.2", NASA Technical Paper 3509, 1995.
4. Spalart, P. R. and Allmaras, S.R., “A One-Equation Turbulence Model for Aerodynamic Flows”, AIAA Paper 92-0439.
5. A. Jameson, W. Schmidt and E. Turkel “Numerical Solution of Euler Solution by finite volume methods with Runge-Kutta time stepping schemes”, AIAA paper 81-1259, January 1981.
6. A. Jameson, “Analysis and Design of Numerical Schemes for Gas Dynamics I : artificial diffusion, upwind biasing, limiters and their effect on accuracy and multi-grid convergence”, International Journal on Computational Fluid Dynamics, 4, 171, 1995.

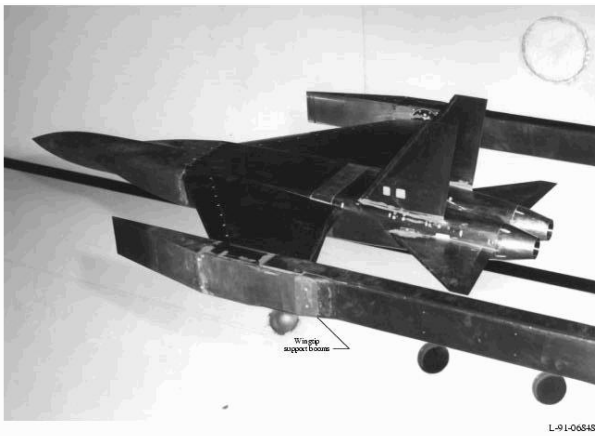

Figure 1 : Photograph of the Model

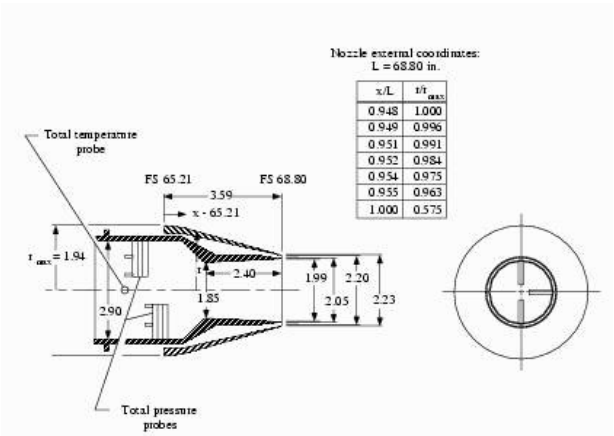

Figure 2: Nozzle Geometric Details

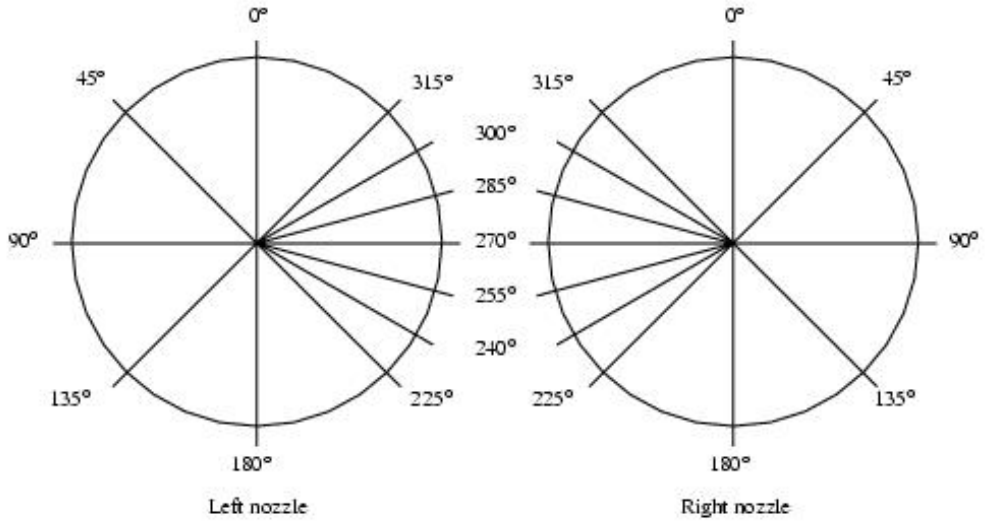

Figure 3 : Circumferential Positions of Pressure Orifice rows for Right and Left Nozzles.

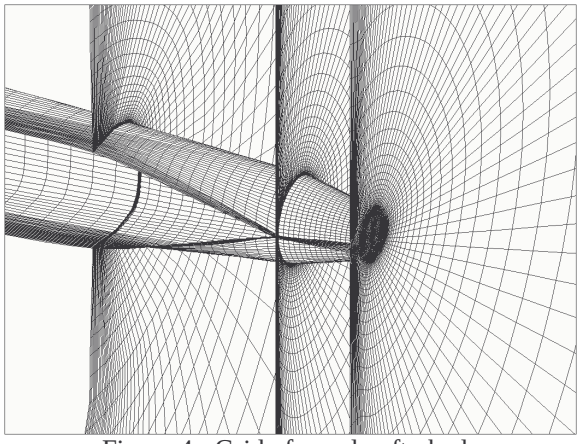

Figure 4 : Grid of nozzle-afterbody

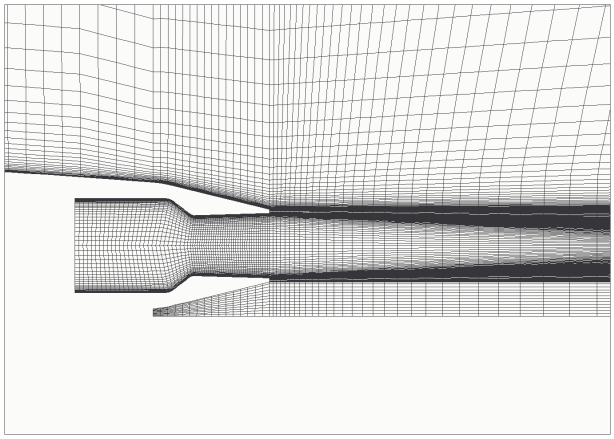

Figure 5 : Grid of nozzle-afterbody

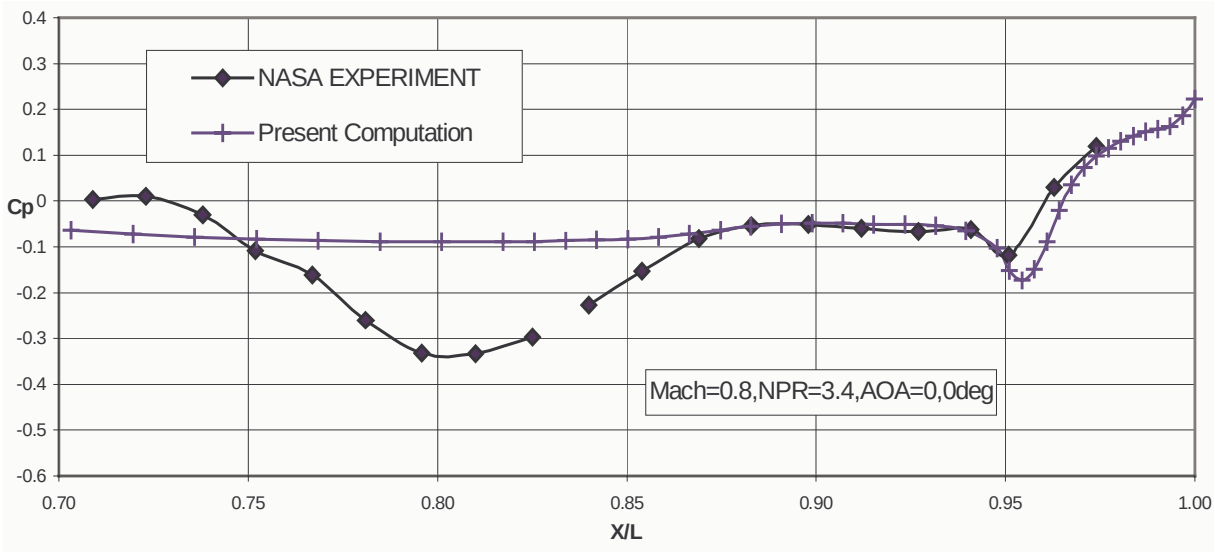

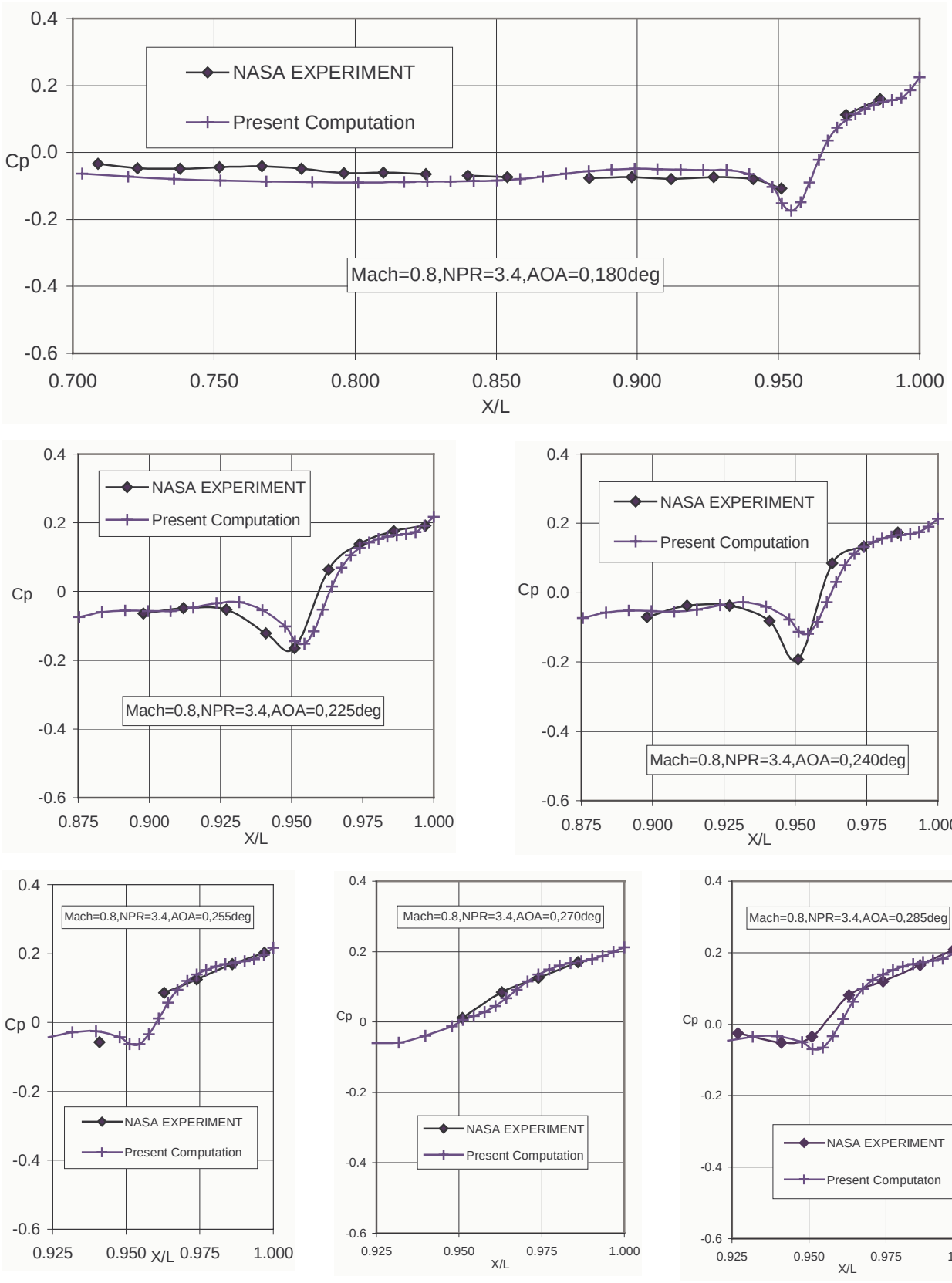

Figure 6: C_P plot for M=0.80, NPR=3.40

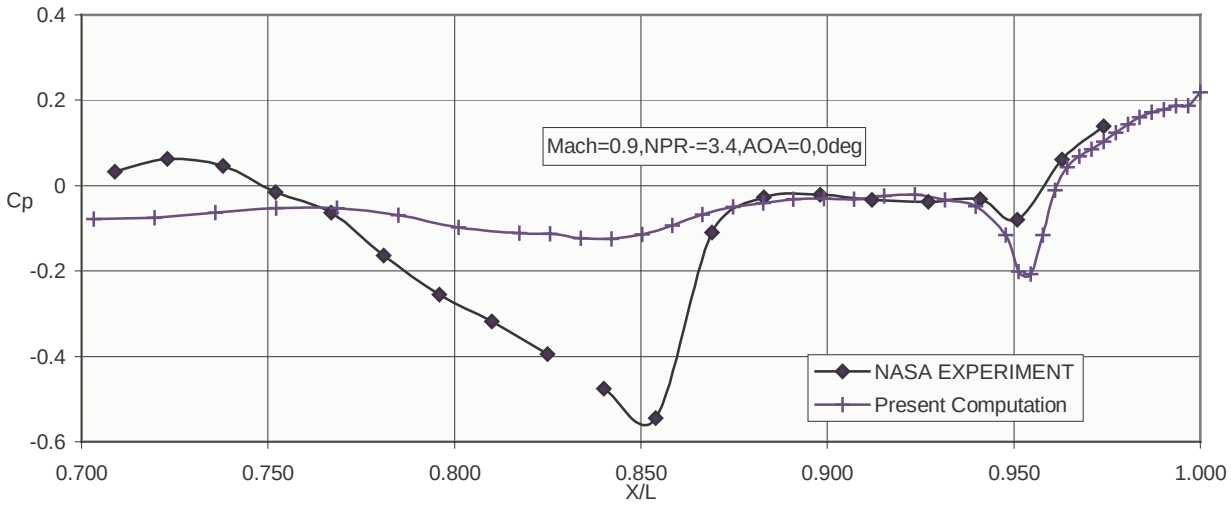
Mach=0.9,NPR-=3.4,AOA=0,0deg
NASA EXPERIMENT
Present Computation
Cp
X/L
0.4
0.2
0
-0.2
-0.4
-0.6
0.700
0.750
0.800
0.850
0.900
0.950
1.000

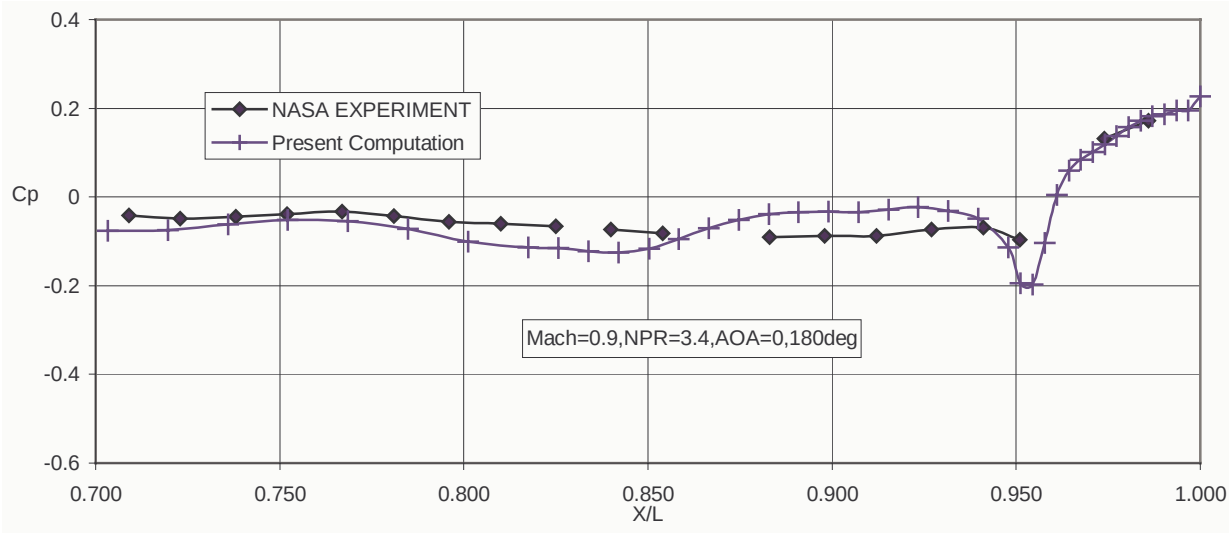
NASA EXPERIMENT
Present Computation
Mach=0.9,NPR=3.4,AOA=0,180deg
Cp
X/L
0.4
0.2
0
-0.2
-0.4
-0.6
0.700
0.750
0.800
0.850
0.900
0.950
1.000

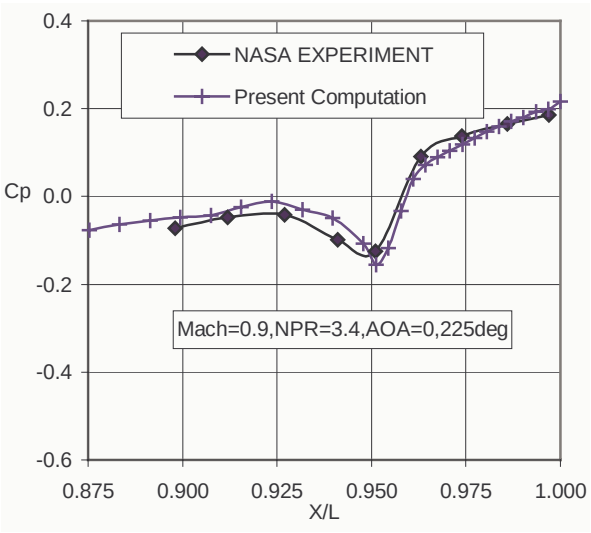
NASA EXPERIMENT
Present Computation
Mach=0.9,NPR=3.4,AOA=0,225deg
Cp
X/L
0.4
0.2
0.0
-0.2
-0.4
-0.6
0.875
0.900
0.925
0.950
0.975
1.000

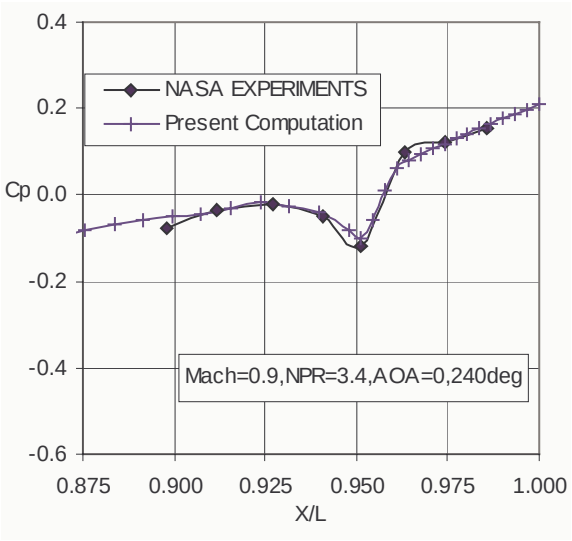
NASA EXPERIMENTS
Present Computation
Mach=0.9,NPR=3.4,AOA=0,240deg
Cp
X/L
0.4
0.2
0.0
-0.2
-0.4
-0.6
0.875
0.900
0.925
0.950
0.975
1.000

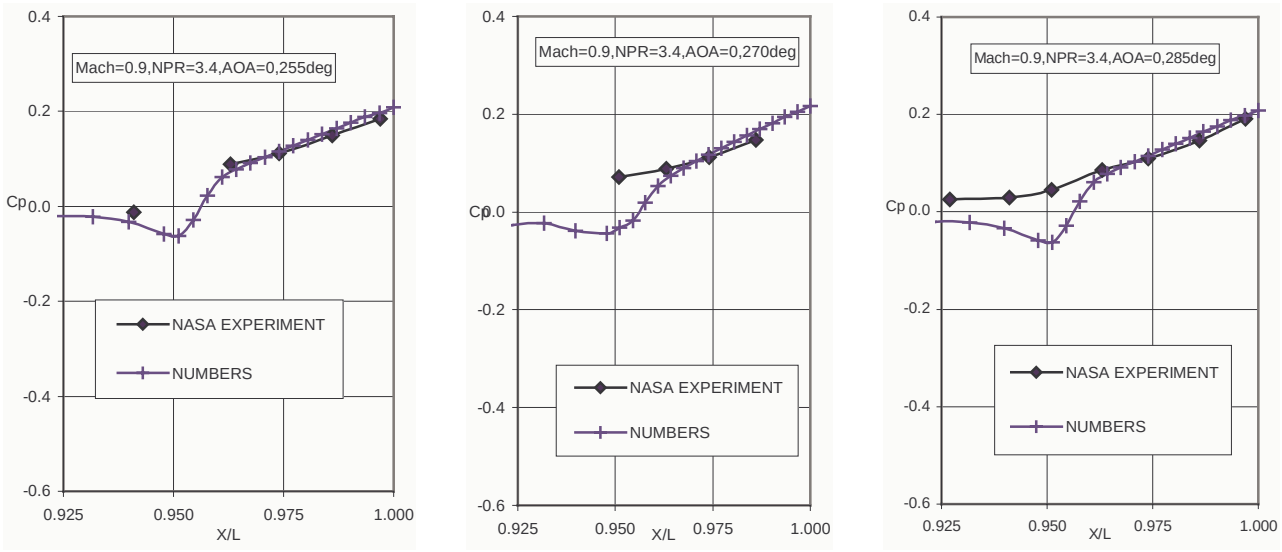

Figure 7: C_P plot for M=0.90, NPR=3.40

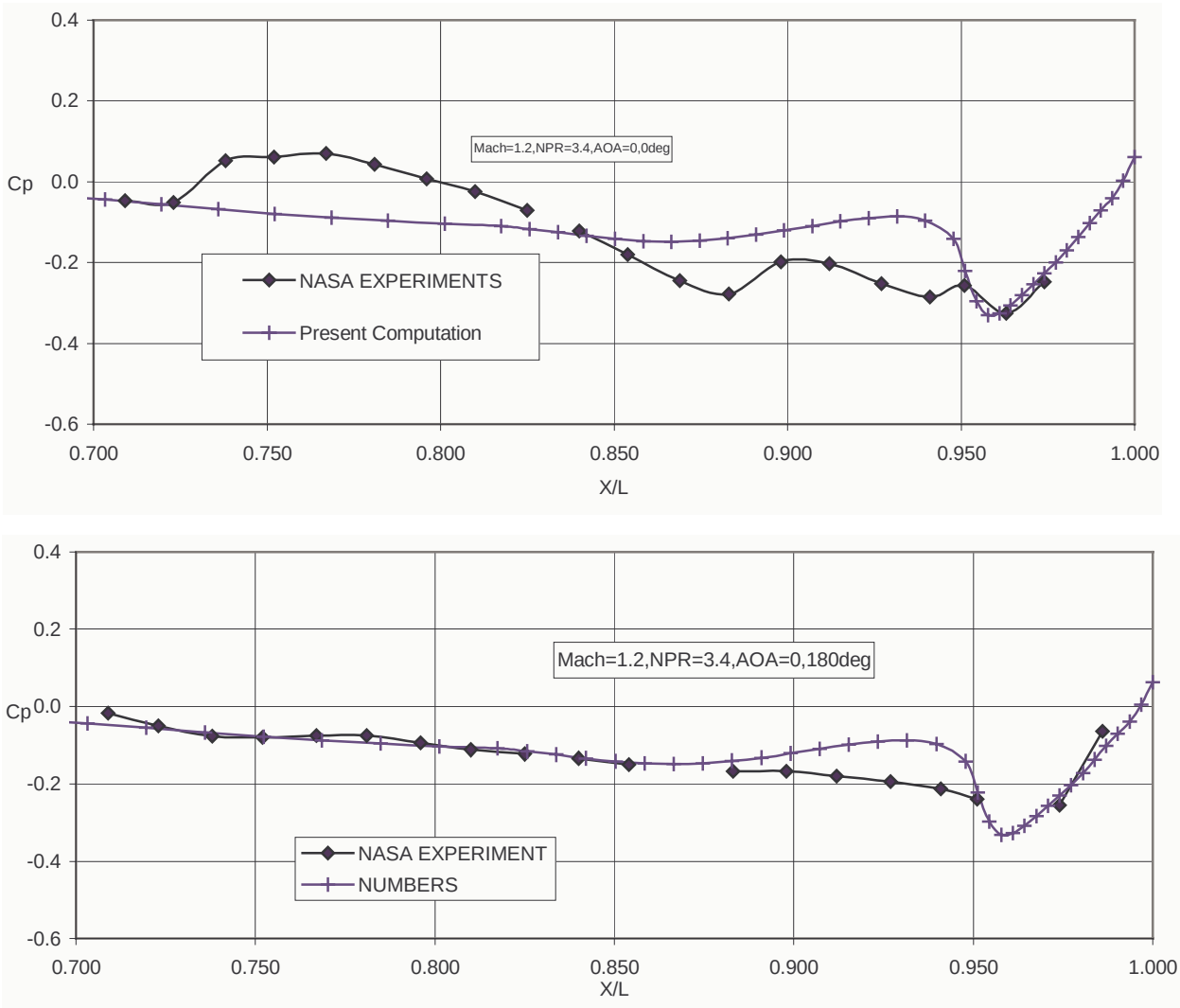

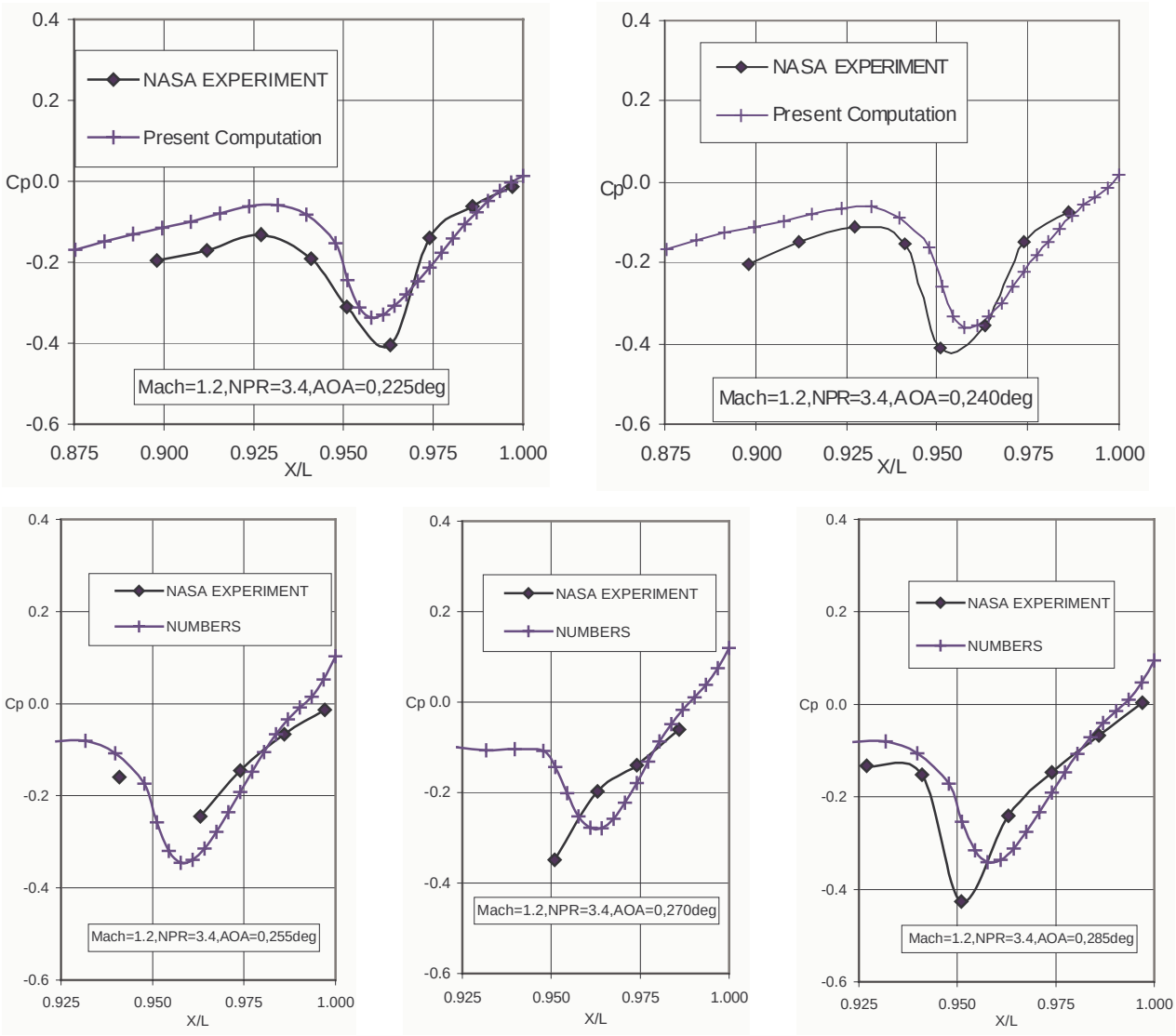

Figure 8: C_P plot for M=1.20, NPR=3.40

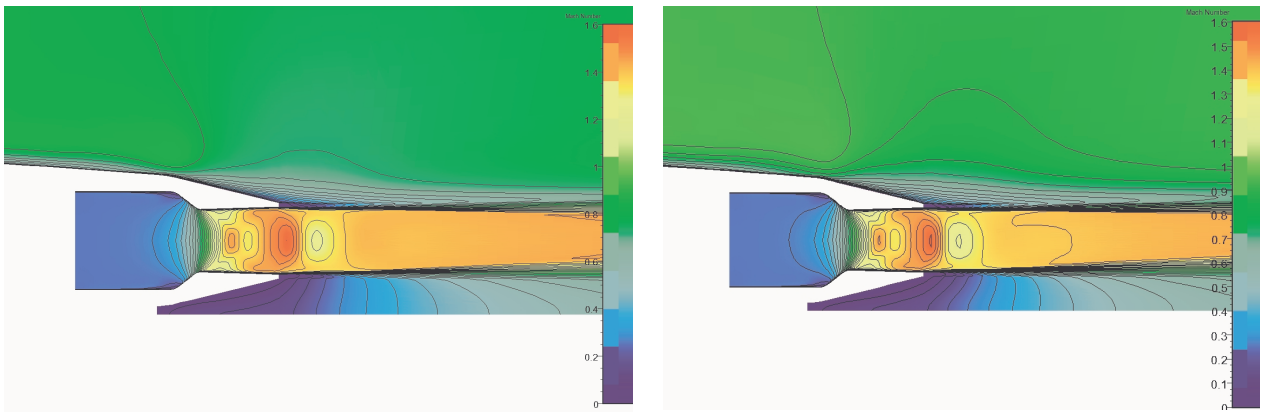

M_∞=0.8, NPR=3.4 M_∞=0.9, NPR=3.4

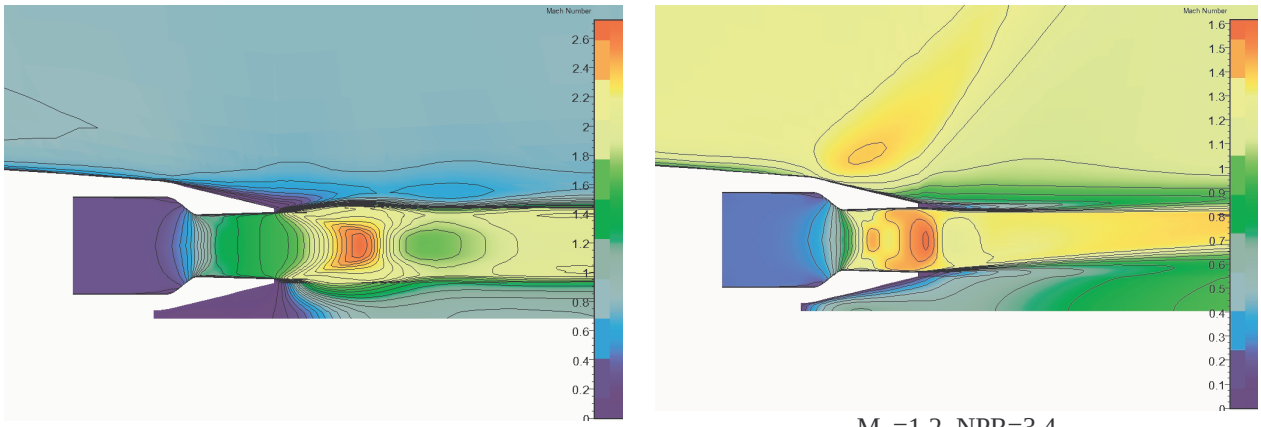

M_∞=0.8, NPR=7.96 M_∞=1.2, NPR=3.4

Figure 9 : Mach Number Plot at Symmetry Plane for Various Cases

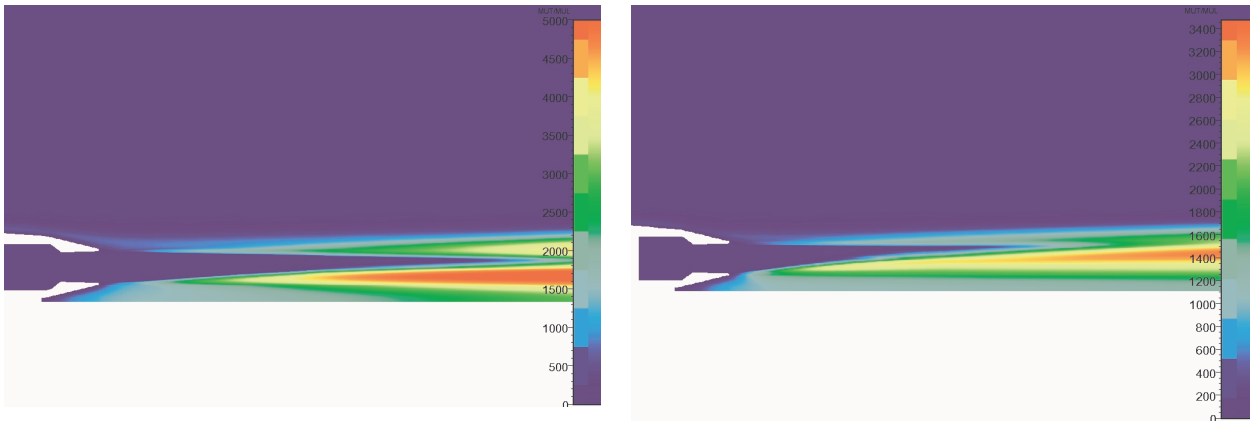

M_∞=0.8, NPR=3.4 M_∞=1.2, NPR=7.8

Figure 10: Turbulent Viscosity Plots for Various Cases

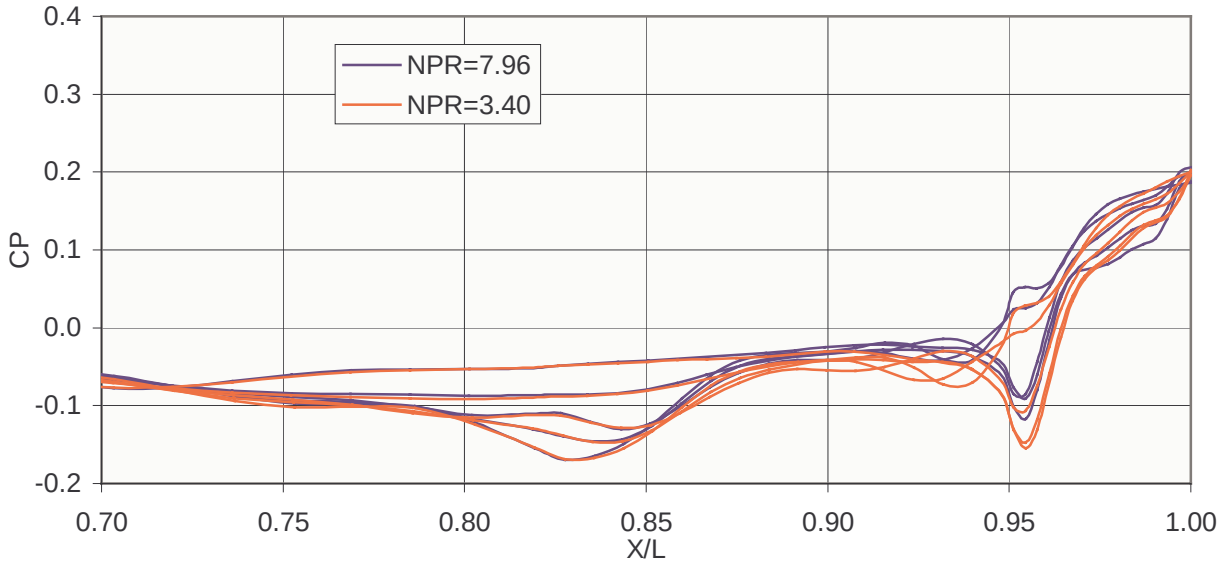

Figure 11: Comparison of C_P Distribution at Mach 0.8

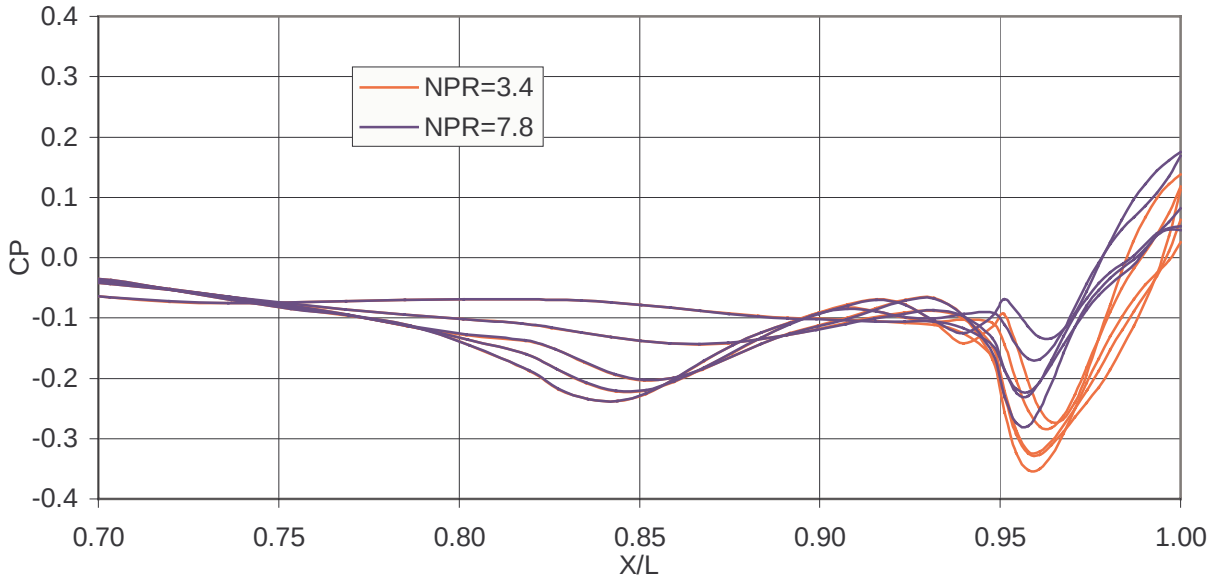

Figure 12: Comparison of C_P Distribution at Mach 1.2

Nomenclature

A_m Maximum Cross Section Area of Model, in ^{2}, 24.57 sq inch
AOA Angle of Attack, degrees
CFL Couranf-Fredricks-Levy Number
C_D Total Afterbody drag coefficient, $\frac{D}{q_\infty A_m}$
C_P Pressure Coefficient, $\frac{(P - P_\infty)}{q_\infty}$
d_{max} Maximum Nozzle diameter at nozzle connect station, 3.88 in
L Length of the model from nose to nozzle exit, 68.8 in
M_∞ Free stream Mach Number
NPR Nozzle Pressure Ratio, $\frac{P_{0,j}}{P_\infty}$
$P_{0,j}$ Total Pressure of the Jet, Pa
P Free stream Pressure, Pa
q_∞ Free stream dynamic pressure, $\frac{1}{2}\rho_\infty V_\infty^2$
Re Reynolds Number,
$T_{0,j}$ Total Temperature of the Jet, K
T_∞ Free stream Temperature, K
V_∞ Free stream Velocity, m/sec
x Axial distance from model nose, in
θ Meredional Angle on nozzles, measured outboard from centerline on top surface, deg
$\alpha_1, \alpha_2, \alpha_3, \alpha_4$ Coefficients of four –step Runge Kutta integration
ρ Density, kg/m^3
ν Molecular kinematic Viscosity, m^2/s
ν_t Turbulent Kinematic Viscosity, m^2/s
Δt time step used in computation